Glass Europe Vol. 2 (2024) 151-164
https://doi.org/10.52825/glass-europe.v2i.2341

Submitted: 11 Sep. 2024 | Accepted: 03 Nov. 2024 | Published: 15 Nov. 2024

Effects of Al Substitution for Fe in $Na_5FeSi_4O_{12}$ (5.1.8) Glasses: Structure and Crystallization

Raine Antonio[1], John Bussey[1,2], Malin C. J. Dixon Wilkins[1], Daniel Neuville[2], Laurent Cormier[3], and John McCloy[1,2]

[1] School of Mechanical and Materials Engineering, Washington State University, Pullman, WA, 99164

[2] Institut de Physique du Globe de Paris, Université Paris Cité, Île-de-France, 75005

[3] Sorbonne Université, Muséum National d'Histoire Naturelle, UMR CNRS 7590, IRD, Institut de Minéralogie, de Physique des Matériaux et de Cosmochimie, IMPMC, 75005 Paris, France

Abstract. In this study, the effects of substituting Al for Fe in $5Na_2O{\cdot}(Al_2O_3)_x{\cdot}(Fe_2O_3)_{1-x}{\cdot}8SiO_2$ glass, x=0 to 1, and $Na_5Al_xFe_{1-x}Si_4O_{12}$ (5.1.8) crystal, were investigated using thermal analysis, Fe K-edge X-ray absorption, X-ray diffraction, Raman spectroscopy, and Electron Probe Microanalysis. In both glass and crystallized glass, nearly all the Fe was tetrahedrally coordinated Fe^{3+}, as expected from the high concentration of Na_2O. The substitution of Al for Fe in the glasses caused the glass transition temperature to increase as polymerization increased, as evidenced by Raman, likely due to both field strength differences of Al vs Fe and a small amount of Fe^{2+} network modifier present with Fe. After heat treatment at 700 °C for 24 hours, the glasses had crystallized, forming Na_2SiO_3 and $NaAlSiO_4$ in compositions with high Al concentrations and the 5.1.8 crystal in compositions with high Fe concentrations. Through electron microprobe, it was determined that <0.04 formula unit Al incorporated into the 5.1.8 crystal, i.e. $Na_5Fe_{0.96}Al_{0.04}Si_4O_{12}$. The 5.1.8 crystal only formed when Fe concentration was higher than Al in the starting glass.

Keywords: $Na_5FeSi_4O_{12}$, $Na_5MSi_4O_{12}$, Crystallized Glass, Glass Structure, Raman Spectroscopy, XANES

1. Introduction

Na, Fe, Al, and Si are among the most common rock-forming elements in the Earth's crust [1] and constitute a significant fraction of some nuclear wastes and immobilized waste forms, including at the Hanford Site in Washington State in the USA [2], [3]. As such, understanding their behavior in silicate melts and glasses is critical for both magmatic processes and nuclear waste vitrification [4], [5], [6].

The $Na_5FeSi_4O_{12}$ phase was first observed in 1930 by Bowen *et al.* [7] while investigating the Na_2O – Fe_2O_3 – SiO_2 system and was labeled 5.1.8 based on component ratios (Na_2O:Fe_2O_3:SiO_2). While initially thought to be comprised of a binary mixture of two phases [7], Ahmadzadeh *et al.* [8] identified the crystal structure using single crystal X-ray diffraction as being trigonal with multiple Na channels. The 5.1.8 crystal structure forms from a framework of $Fe^{3+}O_6$

octahedra, SiO_4 tetrahedra, and a range of NaO_x polyhedra. There are eight distinct Na sites within the crystal with a variety of coordination environments, four of which are partially occupied and highly disordered. $Si_{12}O_{36}$ silicate rings form channels that hold some of the Na polyhedra. Other isostructural phases were documented by Maximov *et al.* [9] in 1974, including $Na_5ScSi_4O_{12}$, $Na_5ErSi_4O_{12}$, and $Na_5YSi_4O_{12}$. Given the presence of these Na^+ channels, a significant body of research on $Na_5MSi_4O_{12}$-structured materials (where M is a trivalent metal ion) exists, examining their applicability for use in Na-ion battery materials, and there has been a recent resurgence of interest in these materials [10], [11], [12]. Even in 1977, Shannon *et al.* [13], [14] examined $Na_5GdSi_4O_{12}$ as a viable competitor to the NASICON ($Na_{1+x}Zr_2Si_xP_{3-x}O_{12}$, $0 \leq x \leq 3$) family of structures, with sodium mobility competitive to $Na_3Zr_2Si_2PO_{12}$. $Na_5GdSi_4O_{12}$ has also been investigated as a candidate material for the safe replacement of organic liquid Na-ion electrolytes [12].

The Na_2O-SiO_2-Fe_2O_3-Al_2O_3 phase diagram of minerals was studied by Bailey and Schairer in 1963 and 1966 [15], [16]. Similar to aegirine (acmite), $NaFeSi_2O_6$ [17], the $Na_5FeSi_4O_{12}$ composition can easily form as a glass or a crystalline phase [8], with the crystalline phase forming isochemically from the amorphous one. However, unlike other Na-Fe-(Al)-Si oxide phases, such as aegirine and iron-substituted nepheline ($Na(Fe,Al)SiO_4$), the 5.1.8 phase has not been observed in nature. This is likely due to the crystal having a particularly high sodium content, and low aqueous durability [7], [8]. In addition to being of geological interest, related phases in the Na-(Fe)-Al-Si oxide system have been observed to crystallize during the vitrification of nuclear waste, such as nepheline and acmite [17], [18], [19]. Nepheline poses significant concern for nuclear waste vitrification, since its crystallization from borosilicate glasses leaves a less-durable sodium borate enriched residual glass. As such, comprehensive understanding of the crystallization of relevant glass systems is important to support the processing of legacy, current, and future radioactive wastes, which often contain large quantities of iron, aluminum, and sodium.

This work examined the $5Na_2O{\cdot}(Al_2O_3)_x{\cdot}(Fe_2O_3)_{1-x}{\cdot}8SiO_2$ glass, replacing Fe (x=0) sequentially with Al (x=1) and the effects of this composition on isothermal crystallization. The impacts of Al incorporation on the properties of the glass have been examined, including density and glass transition temperature (T_g). Glass structure was evaluated by Raman spectroscopy, and the oxidation state and coordination of Fe was determined from X-ray absorption spectroscopy (XAS) at the Fe K-edge. After annealing to promote crystallization, the crystallized glasses were investigated with powder X-ray diffraction (XRD) and electron probe microanalysis (EPMA), in order to determine phases formed at different ratios of Fe/Al in the glass, and whether incorporation of Al into the 5.1.8 phase occurred.

2. Experimental Procedures

2.1 Synthesis

The glass series was synthesized in 50 g batches, following the stoichiometry $Na_5Fe_{1-x}Al_xSi_4O_{12}$ (x = 0, 0.25, 0.5, 0.75, 1). Compositions are identified by the percentage of Al/(Fe+Al), *e.g.,* 0Al is where x = 0, the Fe end-member. The precursors utilized were Na_2CO_3 (Fisher Lot# 123556), Fe_2O_3 (Alfa Aesar Lot# E16Z021), Al_2O_3 (Fisher Lot# 145426), and SiO_2 (Lot# 08062110 US Silica). Glasses were melted at 1500 °C for 1 h in 90Pt-10Rh crucibles before being poured onto an Inconel® plate to quench to room temperature. Glasses were powdered in a WC ring mill (Angstrom). To form crystallized glasses, 5 g aliquots of each powdered glass were then placed

in porcelain crucibles coated with BN before treatment at 700 °C for 24 h. Selected samples were separately heat treated at 750 °C for 24 h to increase crystallization fraction.

2.2 X-ray Fluorescence (XRF)

Powdered samples were mixed with spectroscopically pure di-lithium tetraborate before being fused for 5 minutes at 1000 °C in a graphite crucible. These melts were poured into graphite molds to form beads. The beads were then comminuted in a swingmill for 35 seconds and fused again under the same conditions. The samples were then flattened using 600 grit sandpaper and cleaned of impurities in an ultrasonic bath. A Rigaku 3370 XRF Spectrometer was used for XRF measurements with a Rh target (50 kV/50 mA) and a 25 mm mask for all elements.

2.3 Pycnometry

Density measurements were obtained with a Micromeritics AccuPyc II 1340 Gas Pycnometer in a 3.5 cm^3 sample holder. Ten measurements were taken for three aliquots of each sample with an inlet pressure of helium at 19.5 – 20.5 psi.

2.4 Thermal Analysis

Differential thermal analysis (DTA) was performed utilizing an SDT Q600 (TA Instruments) to determine the glass transition temperatures (T_g). Less than a gram of glass was heated in 90Pt-10Rh crucibles under an inert N_2 atmosphere up to 1200 °C at a rate of 10 °C·min^{-1}. T_g was determined by the onset method.

2.5 Raman spectroscopy

Unpolarized Raman spectra were acquired using a 488 nm (Coherent MX) laser focused through a 50X objective (Olympus) and a Labram HR Evolution spectrometer (Horiba) equipped with a Peltier-cooled CCD and 1800 lines per mm grating. 600 mW laser power at the source, ~1.7 cm^{-1} spectral resolution, ~1 µm spatial resolution, and an Ultra Low Frequency filter were used to collect spectra from 20 cm^{-1} – 1600 cm^{-1}. Spectragryph [20] was utilized for spectra visualization and to normalize all spectra to the feature at 1070 cm^{-1}. There were no observed burn marks on the samples after being measured.

2.6 X-ray Absorption Spectroscopy

The Fe K-edge X-ray Absorption Near Edge Structure (XANES) spectra were measured at the ODE beamline [21] at the SOLEIL synchrotron facility (Saint-Aubin, France) operating at 2.72 GeV and 450 mA. XANES were collected in dispersive transmission mode using a bent Si(111) polychromator and a Princeton CDD camera. The conversion from pixel to energy was obtained by polynomial fitting of a reference Fe foil. Spectra were collected from 7100 eV to 7200 eV, with a resolution of 0.2 eV. A macro beam of 100 × 100 $µm^2$ was used to minimize photo-oxidation of the samples. All XANES spectra were processed using the Larch software [22]. The pre-edge feature was analyzed by determining its centroid position and integrated intensity, which were derived from pre-edge fitting using pseudo-Voigt functions. These results were compared to the centroid-area diagram previously established by Wilke [23], [24].

2.7 X-Ray Diffraction

X-ray diffraction (XRD) patterns were collected with a PANalytical X'Pert Pro MPD diffractometer utilizing Fe-filtered Co K_α radiation. Rietveld refinements were performed with a standard procedure using the GSAS-II software package [25]. Amorphous fraction was determined by adding a precisely measured known quantity of an internal standard (high purity Al_2O_3) before measurement.

2.8 Electron probe microanalysis

A piece of the heat-treated 50Al sample, 750 °C for 24 hours, was mounted in epoxy, ground with silicon carbide and oil up to 1000 grit, then polished to 1 µm with a diamond suspension in oil (oil was used to prevent leaching of any water-soluble phases). 50Al treated at 750 °C was chosen since it was the crystallized glass sample synthesized with likely the highest Al incorporation into 5.1.8 (highest Al content and highest treatment temperature). Significant phase assemblage changes from 50Al 700 °C are not expected. Compositions of 5.1.8. crystals, located by backscatter electron (BSE) imaging in a scanning electron microscope (SEM), were measured with a JOEL JXA-8500F field emission electron microprobe (EPMA), equipped with five wavelength-dispersive X-ray spectrometers (WDS). 15 kV accelerating voltage, 5 µm spot size, 10 mA beam current, and a 40° takeoff angle were used. Element specific conductions include: for Na, 20 s peak count times with a TAP analyzer crystal and Albite #4 (C.M. Taylor Corp.) standard; for Fe, 40 s count, LIFH analyzer, K-411 (NIST) standard; for Si, 20 s count, PETJ analyzer, K-411 (NIST) standard; for Al, 20 s count, TAP analyzer, K-412 (NIST) standard. Probe for EPMA [26] was used for analysis.

3. Results and Discussion

3.1 Glasses

There was no visually observed crystallization within the glasses upon pouring. The colors of the bulk glasses varied from reddish green for 0Al to off-white for 100Al. On examining the XRD patterns of the quenched samples, a small amount of unreacted sodium carbonate was seen in all glass samples. As there was a large amount of sodium carbonate added as a precursor, the trace sodium carbonate could be residual caused by only melting for one hour, with no stirring being applied to the melts and no borate component to drive a primary melt [27]. Glass samples were not remelted, as Na_2CO_3 decomposition was not observed in TGA, Rietveld refinement found less than 1% of the crystallized glass composition was Na_2CO_3, and high melting temperatures and/or longer melting times were expected to cause Na volatilization.

***Table 1**. As batched mol% composition, XRF measured mol% composition (normalized to 100%), XRF weight % measured total impurities, and bulk glass densities determined by pycnometry. Error on XRF measurements calculated based on [28] and rounded up to the nearest tenth. Due to rounding, totals may not add to 100.0%.*

		Na_2O (mol%)	**Fe_2O_3 (mol%)**	**Al_2O_3 (mol%)**	**SiO_2 (mol%)**	**Al/(Fe+Al) (molar)**	**Na/(Fe+Al) (molar)**	**Total Impurity (wt.%)**	**Density (g/cm^3)**
0Al	Batched	35.7	7.1	0.0	57.1	0	5.00	-	-
	Measured	34.4±0.1	6.7±0.1	0.3±0.6	58.6±0.1	0.04	4.90	0.1±0.1	2.64±0.01
25Al	Batched	35.7	5.4	1.8	57.1	0.25	5.00	-	-
	Measured	34.4±0.1	5.4±0.1	2.1±0.1	58.1±0.1	0.28	4.64	0.1±0.1	2.57±0.01
50Al	Batched	35.7	3.6	3.6	57.1	0.50	5.00	-	-
	Measured	34.7±0.1	3.5±0.1	3.8±0.1	57.9±0.1	0.52	4.70	0.1±0.1	2.43±0.01
75Al	Batched	35.7	1.8	5.4	57.1	0.75	5.00	-	-
	Measured	33.5±0.1	1.8±0.1	5.7±0.1	59.0±0.1	0.76	4.71	0.1±0.1	2.45±0.01
100Al	Batched	35.7	0.0	7.1	57.1	1.00	5.00	-	-
	Measured	35.0±0.1	0.0±0.4	7.3±0.1	57.6±0.1	1.00	4.76	0.0±0.1	2.40±0.01

The compositions of the produced glasses were examined using quantitative X-ray fluorescence spectroscopy (XRF), see Table 1. The batched and measured compositions largely matched, indicating limited volatilization during melting. The largest losses were in Na_2O, as expected [29]. In all cases, the $Al_2O_3/(Fe_2O_3+Al_2O_3)$ ratio was within 0.04 of the targeted composition. The small amount of Fe in the 100Al sample is impurity from the SiO_2 and/or Al_2O_3 precursor. No other major characteristic lines beyond those from the batched elements were observed, and impurities totaled 0.1 wt% or less, mostly from the Fe_2O_3 precursor (TiO_2, MnO, P_2O_5, Cr_2O_3, NiO, CuO, ZnO). When accounting for loss on ignition (LOI, measured during the XRF bead synthesis process), weight % measured totals for all samples were within ± 0.1 of 100.0. LOI values ranged from 4.5 to 6.4 weight %, and are likely due to loss of adsorbed water, as well as possible decomposition of residual carbonate.

As the relative fraction of Al in the glass increased, a corresponding decrease in the bulk glass density was observed. The decrease in density is perhaps from Al being a lighter element than Fe, although a slight increase in molar volume (peaking at 50Al) remains unclear. While the precision was at most 0.002 g/cm^3, accuracy for this measurement is on the order of 0.01 g/cm^3.

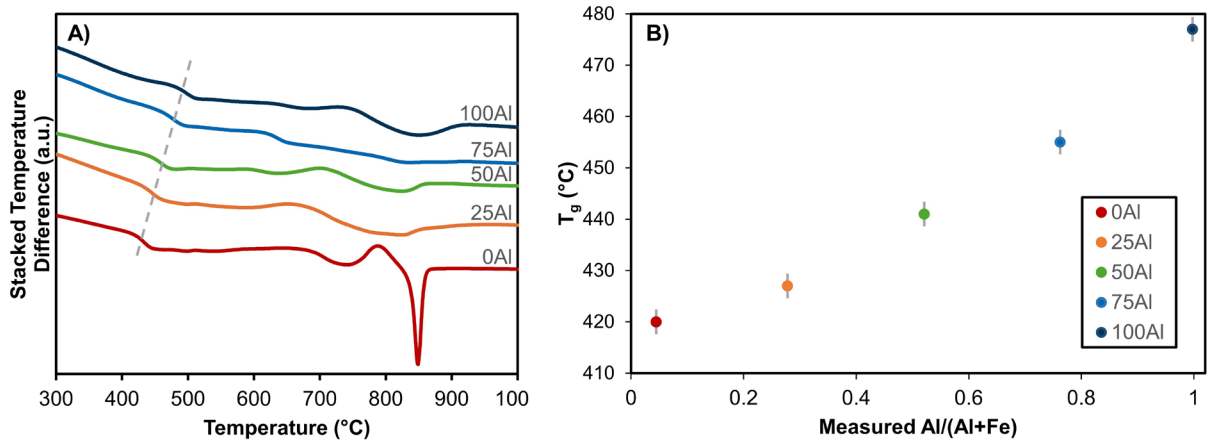

Figure 1. *A) Raw differential thermal analysis (DTA) traces collected at a 10°C min^{-1} heating rate. Glass transition marked with gray dotted line. B) Onset glass transition temperatures (T_g) determined by DTA; compositions based on XRF. T_g error calculated to be ±3 °C from a 95% confidence interval constructed using Student's t-distribution on triplicate onset calculations from triplicate measurements with the same parameters used herein on the base glass from [30].*

Using differential thermal analysis (DTA), the onset glass transition temperature (T_g) was determined for each glass (Figure 1). The T_g fell between 420 °C and 480 °C and with an apparently non-linear increase in T_g observed as Al replaces Fe. This is likely due to the higher field strength of Al compared to Fe. A secondary mechanism for the increasing T_g is the increase in Si network polymerization as Al replaces Fe, with the cause potentially being related to the presence of some Fe^{2+} (see below Raman and XAS). Another potential contribution to the increased T_g is the addition of Al which, along with Fe^{3+} in our case, requires Na to play a charge-compensating role [31]. Broad crystallization and melting features are observed in 100Al, 50Al, and 25Al, while there is minimal evidence of crystallization in 75Al (consistent with diffraction data, section 3.2). In 0Al, sharper crystallization and melting features are observed, at temperatures consistent with previous reports [8]. The difference in sharpness is likely due to the difference in isochemical vs mixed crystallization, while the melting peak areas appear roughly proportional to diffraction results.

To examine the impact of the Fe/Al ratio on the structure of the glass network, Raman spectra were collected on bulk samples of each glass (see Figure 2A). Each of the glasses has a Boson peak around 90 cm^{-1}. The broadness and frequency of the boson peak increase minorly with Fe addition, possibly due to an increase in SiO_4 tetrahedral distortion [32]. The several peaks present in the medium frequency range (400 cm^{-1} to 800 cm^{-1} here) can be assigned to a variety of modes, including bending of Si-O-Si bonds. Similar spectra have been observed in similar Al-only [33] and Fe-only [34] compositions, with the intermediate spectra containing features of both.

The high frequency Raman envelope contains three defined peaks between 800 cm^{-1} and 1200 cm^{-1}, corresponding to stretching vibrations of networking forming silicates in varied levels of polymerization (several Q^n species, where n is the number of bridging oxygens on the SiO_4 tetrahedron). The lowest frequency feature goes from minor to dominant with addition of Fe and the highest frequency feature can be separated into two peaks. To better elucidate the differences in Q^n speciation, difference spectra (Figure 2B) were prepared, comparing each spectrum to that of 100Al. The largest increase with Fe addition from the Al endmember was in a spectral contribution centered around 890 cm^{-1}, while a smaller spectral contribution centered at 950 cm^{-1}

also increased, and a spectral contribution at 1120 cm^{-1} decreased. These three contributions are assigned to contributions from Fe^{3+}-O-Si units [34] overlapping with Q^1, Q^2, and Q^3, respectively. No significant changes were observed in the band assigned to T_{2s}. Significant contribution of Q^0, and Q^4 are not observed in any of the Raman spectra (to reinterpret the peak deconvolution from [8]), consistent with an equilibrium between $2Q^2 \Leftrightarrow Q^1+Q^3$. As Al is substituted for Fe, there appears to be a higher contribution of Q^3 units and lower contribution of Q^2 units, indicating that the substitution of Al for Fe into the glass matrix increases the silicate network polymerization. No significant changes in the Q^2 and Q^3 contributions in 75Al are observed compared to 100Al. Further, with more Fe, the strength of the Fe^{3+}-O-Si contribution increases drastically, agreeing with previous studies [35]. Together these results indicate that Fe has more modifying behavior compared to the more networking forming behavior of Al in this system. While most Fe is expected to be Fe^{3+} from the XAS data discussed below, there is likely some Fe^{2+} in the glass matrix acting as a network modifier and in turn decreasing polymerization. This could explain the minor variations in Q^n speciation, becoming slightly more depolymerized as Fe is added, some of which is Fe^{2+} so behaving like a network modifier. Likewise, this increased polymerization could be connected to Al more strongly requiring Na charge compensation compared to Fe^{3+}.

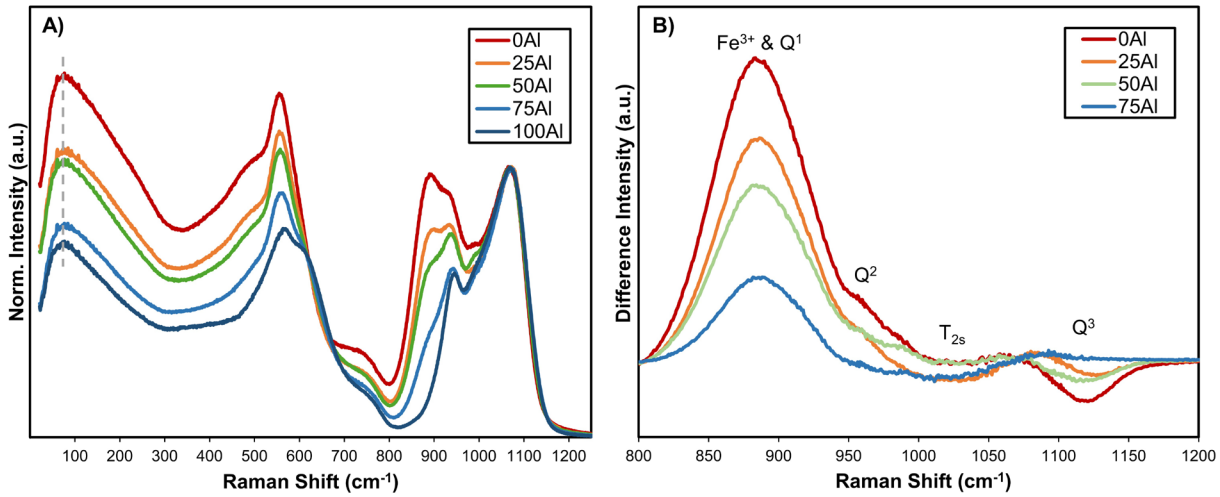

Figure 2. *A) Raman spectra of glasses in the Na-Fe-Al-Si oxide system, normalized to the intensity at 1070 cm^{-1}: B) Difference of normalized high frequency bands from the 100Al spectra with annotated spectral contribution assignments.*

Fe K-edge XANES was utilized to examine the oxidation state and coordination environment of Fe in these glasses (Figure 3). Minimal change was observed across the series (Figure 3A) and the data resembles that of many silicate glasses [17], [36]. The pre-edge feature contains a single peak at 7114 eV. This is consistent with the features of oxidized Fe in glass [24]. Plotting of pre-edge centroid position and integrated intensity (Figure 3B) and comparing to reference compounds of known Fe oxidation state and coordination environments [23], [24], it is apparent that the vast majority of Fe is present as tetrahedrally coordinated Fe^{3+} in glasses from this study. This suggests that the Fe in these glasses is acting primarily as a network former, which is in good agreement with Tuheen *et al.* [36] whose computational work calculated that 93% of the Fe in 5.1.8 glass should be Fe^{3+} with an average coordination of 4.14. The only potential trend from the pre-edge analysis is a very slight decrease in Total Integrated Intensity with increasing Fe. However, as Al is substituted for Fe, pre-edge analysis does not suggest any substantial change

to the Fe coordination or oxidation state. As discussed previously in [17] and references therein, extraction of very precise values of Fe redox is complicated by monochromator resolution limits, and with the best practices, a Fe pre-edge centroid energy uncertainty of no better than ±0.1 eV is achievable. However, with glasses synthesized in air at 1500 °C (as those here), the relation given in Sack et al. [37] predicts 95% Fe^{3+} for the stoichiometric 5.1.8 (0Al), while synthesis temperatures as high as 1250 °C in air predict 99% Fe^{3+} due to the large Na/Fe ratio in the starting composition. Previous comparisons made in other sodium iron silicate glasses between XAS Fe pre-edge, Mössbauer, and wet chemistry have shown very similar values, though absolute quantification remains slightly more problematic for XAS [17]. Our previous Mössbauer study on 5.1.8 glass [8] suggested 90% tetrahedral Fe^{3+} with the remaining being 5- or 6-coordinated Fe^{2+}, and wet chemistry suggested 93% Fe^{3+}, consistent with the current study and the chemical model redox expectations.

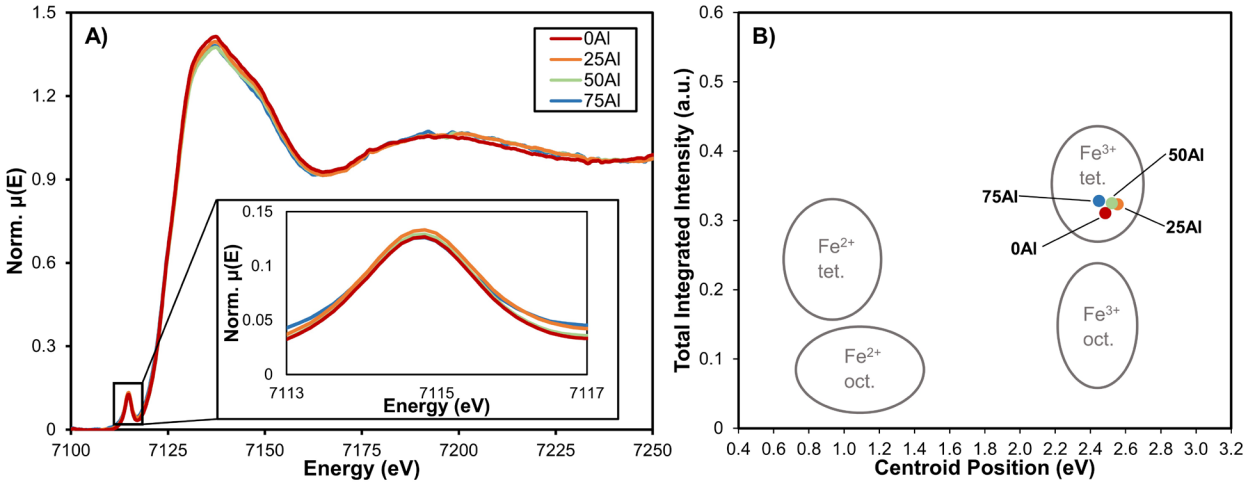

Figure 3. *Fe K-edge XAS spectra. A) XANES spectra of quenched samples containing Fe. Pre-edge enlarged in inset. B) Centroid position at 7112 eV and integrated intensity from pre-edge fitting. Regions for typical oxidation and coordination redrawn based on Wilke et al. [23], [24].*

3.2 Crystallized glasses

The 5.1.8 phase ($Na_5FeSi_4O_{12}$, space group $R\bar{3}c$, ICSD # 96-202-1333) was present in the heat-treated materials with an Fe:Al ratio of up to 50:50 (*i.e.,* 0Al, 25 Al, 50Al), with the relative abundances decreasing as the amount of Al in the initial glass increased (Figure 4, Table 2). Orthorhombic sodium metasilicate (Na_2SiO_3, space group $Cmc2_1$, ICSD # 01-072-0079) was the dominant crystalline phase present in 75Al and 100Al and was also present in 50Al. Hexagonal nepheline ($NaAlSiO_4$, space group $P6_3$, ICSD # 96-400-2836) is prominent in the 100Al sample devoid of Fe and trace quantities were also observed in 25Al and 75Al. The lattice parameters of 5.1.8 and nepheline were not observed to significantly change with different amounts of Al and Fe in the glass. A small change in nepheline lattice parameters indicating Fe incorporation cannot be ruled out, however, due to the small amounts of nepheline present in 75Al and 25Al. Diffraction cannot rule out the presence of Fe-rich nanoclusters, sometimes observed in Fe-rich peralkaline melts, which if present, would likely affect the phase assemblage and other properties.

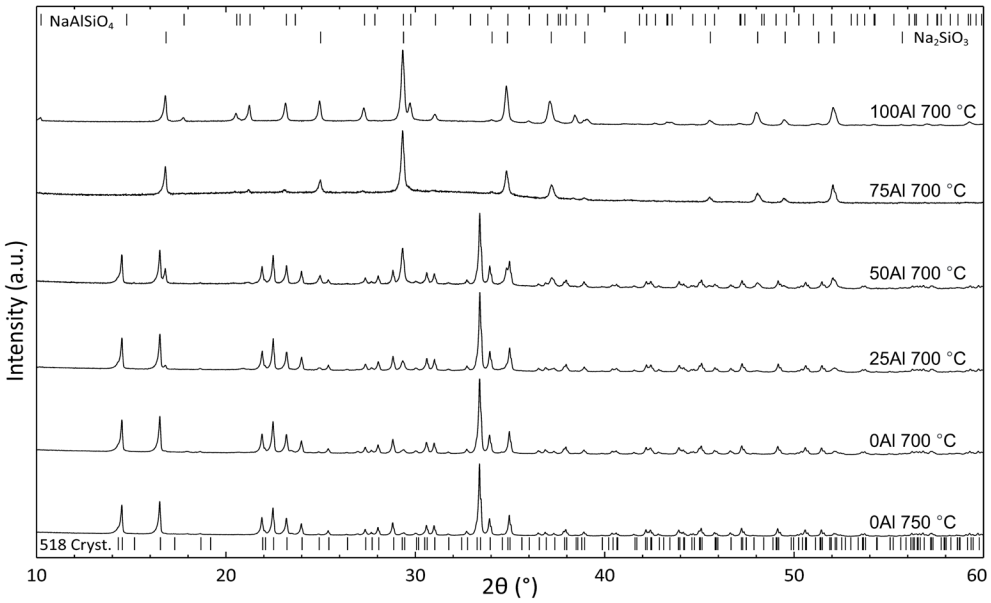

Figure 4. *X-ray diffraction patterns collected with Co K_α X-rays.*

Table 2. *Rietveld refinement (wt.%), error was rounded up to nearest 0.1.*

T (°C)	Name	5.1.8	$NaAlSiO_4$	Na_2SiO_3	Amorphous
750	0Al	69.6±0.3	-	-	30.4±0.1
700	0Al	64.9±0.3	-	-	35.1±0.1
700	25Al	55.6±0.2	1.2±0.1	-	43.1±0.1
700	50Al	31.2±0.3	-	6.4±0.1	62.4±0.1
700	75Al	-	0.9±0.1	6.2±0.1	92.9±0.1
700	100Al	-	14.1±0.1	19.9±0.1	66.1±0.1

As Al increased in the glass, the crystallized samples showed an increase in the observed fractions of nepheline and sodium silicate, as well as a general trend of increasing amorphous content. The observed amorphous fraction was highest for 75Al (92.9 wt.%), with 100Al containing significantly higher fractions of $NaAlSiO_4$ and Na_2SiO_3 (14.1 wt.% and 19.9 wt.%, respectively, compared to 0.9 wt.% and 6.2 wt.% for 75Al). Given that this is the material with the lowest Al incorporation that did not form any crystalline 5.1.8, it is apparent that higher Al contents destabilize 5.1.8, making a phase assemblage with a significantly higher amorphous fraction more stable under these conditions. Having some Fe also appears to stabilize the glass and inhibit $NaAlSiO_4$ and Na_2SiO_3 crystallization. This is notable as it disagrees with past studies that show moderate levels of Fe should increase $NaAlSiO_4$ growth [1], although the compositions studied here contain considerably more Na_2O. The increased levels of Na appear to have changed the ideal Fe:Al ratio for $NaAlSiO_4$ formation. It is possible that the high amount of Na reduces the amount of Fe^{2+} and thus limits the nucleation of magnetite spinel (Fe_3O_4), which is thought to play a role in the nucleation of $NaAlSiO_4$ [38]. Without forming magnetite, the Fe only inhibits $NaAlSiO_4$ by reducing the amount of available Al, instead of promoting it like in other systems. Given that in this compositional space most of the Fe (see above) and all of the Al (per ^{27}Al Nuclear Magnetic Resonance, [31]) are expected to be trivalent with four-fold coordination and are similarly sized, the differences in glass structure, crystallization, and resulting properties are perhaps surprising,

although have been noted previously [1], [15], [16], [34]. Ionic radii and field strength differences as well as minor presence of Fe^{2+} offer explanations for the differences across the 5.1.8 Fe-Al join.

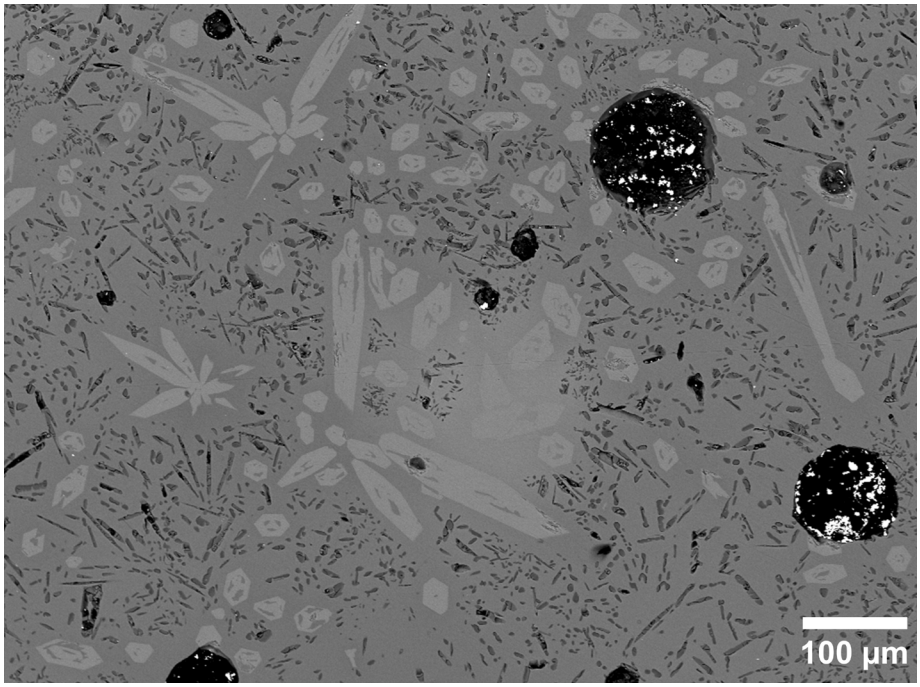

Figure 5. *SEM-BSE micrograph of 50Al crystallized at 750 °C; observed phases: 5.1.8 – light gray larger crystals, Na_2SiO_3 – dark gray smaller crystals, glass matrix – neutral gray/background, porosity – black.*

Electron micrographs (SEM-BSE) provided evidence for the phase assemblage identified by XRD (Figure 5). Grains of 5.1.8 (brighter due to higher average Z, since $Z_{Fe} > Z_{Al}$) formed as large 10 – 100 µm euhedral laths, many of which are skeletal, containing inclusions of uncrystallized glass. These crystals resemble hexagonal rods, and at times originate from a central location, creating "flower like" patterns, presumably due to their nucleation from a single point. Na_2SiO_3 was observed as significantly smaller grains, approximately 5 – 10 µm in "needle like" morphologies. Na_2SiO_3 was observed to be depleted around 5.1.8 grains, presumably due to competition for Na and Si. This implies that the 5.1.8 crystallized at small undercoolings from the liquidus (skeletal morphology [39]), rejecting Al at the interface, likely before the crystallization of the sodium metasilicate. Some regions of porosity are observed, consistent with the process of production of these materials, where powdered glass was heated above T_g, but below the temperatures needed for low viscosity flow.

Table 3*. EPMA Measurement of 5.1.8 from 50Al Crystallized at 700°C.*

Composition (on the basis of 12 oxygens)	**Na**	**Fe**	**Si**	**Al**	**O**
$Na_{4.85}Fe_{0.99}Al_{0.04}Si_{4.02}O_{12}$	4.85	0.99	4.02	0.04	12.00
Error (1-sided 95% Confidence Interval from Student's t-distribution)	0.20	0.02	0.05	0.00	-

Electron Probe Micro Analysis was performed on 5.1.8 crystals in 50Al heat treated at 750 °C, the highest Al content glass which formed measurable 5.1.8 by XRD, to identify the extent of Al incorporation in this phase. Measured Al in the 5.1.8 crystal was 0.2 mol.%, leading to a measured composition of $Na_{4.85}Fe_{0.99}Al_{0.04}Si_{4.02}O_{12}$ (Table 3). This result agrees with XRD, as there is no significant shift in the unit cell parameters of the 5.1.8 crystal when crystallized from glasses containing or lacking Al_2O_3. Al incorporation into the 5.1.8 crystal may be affected by the relatively smaller size of Al^{3+} compared to Fe^{3+} (ionic radii: 0.54 Å for Al^{3+} and 0.65 Å for Fe^{3+} [40]), as the 5.1.8 structure apparently favors larger trivalent cations like trivalent rare earths. According to Shannon *et al*. [13], in $Na_5MSi_4O_{12}$ crystals the ionic radii of M has a direct impact on the space between the $Si_{12}O_{36}$ rings, and Al^{3+} perhaps would create too small of an inter-ring distance for formation of this structure.

4. Conclusions

In this study, the effects of different ratios of Al and Fe were investigated on the formation of $Na_5FeSi_4O_{12}$ through the process of glass fabrication then crystallization. The glasses were characterized using thermal analysis, pycnometry, XANES, and Raman. Increasing the Al in the glass increased the silicate network polymerization and glass transition temperature and decreased the density of the glass. Iron occurs as tetrahedrally coordinated Fe^{3+} and stabilizes the glass from crystallization, inhibiting $NaAlSiO_4$ and Na_2SiO_3 crystal growth. Within the crystallized glasses, there is very little incorporation of Al into the 5.1.8 crystals. This is likely due to the difference in size between Al and Fe, as the two elements have the same trivalent oxidation state and four-fold coordination number in the glass. Iron chemistry in a high sodium environment is important to understand for formulation of certain nuclear waste glasses. Given the similar roles for Al and Fe^{3+} in the network, the role of <10% of Fe as Fe^{2+} has a measurable effect on the observed polymerization of the glass, and likely affects the glass transition as well.

To better understand the role of Al in the glass, future studies should investigate the glass viscosity change in this series, potentially as a function of imposed redox. As an example, research into iron's changing role in $NaAlSiO_4$ formation based on Na content could be investigated by crystallizing multiple sodium aluminosilicate glasses with a ratio 75Al:25Fe and decreasing Na amounts. The morphology of the crystallized glasses and the sequence and kinetics of the crystalline phase evolution, particularly in the 50Al composition with the largest diversity of phases, could offer additional insight on potential control of the crystallization.

Data availability statement

Data will be made available upon request.

Author contributions

RA: Investigation, Writing – original draft, Writing – review & editing. JB: Investigation, Writing – original draft, Writing – review & editing. MCJDW: Investigation, Writing – original draft, Writing – review & editing. DN: Investigation, Writing – review & editing. LC: Investigation, Writing – review & editing. JM: Conceptualization, Resources, Supervision, Funding acquisition, Project administration, Writing – review & editing.

Competing interests

The authors declare that they have no competing interests.

Funding

RA, JB, and JM acknowledge funding from US Department of Energy, Office of Environmental Management, through the Office of River Protection, Waste Treatment and Immobilization Plant Federal Project Office, contract number 89304022CEM000015 under the direction of Dr. Albert A. Kruger.

Acknowledgement

The authors thank Scott Boroughs, Ashley Steiner, and Sam Karcher for helpful discussions. XRF and EPMA were performed at the Peter Hooper GeoAnalytical Lab at WSU. We thank SOLEIL (Gif-sur-Yvette, France) for provision of synchrotron facilities (project numbers 20221659) as well as Lucie Nataf for her help on the ODE beamline. Raman spectroscopy was performed at the Institut de Physique du Globe de Paris (IPGP). The insightful comments of two reviewers improved this manuscript.

References

[1] M. Ahmadzadeh, J. Marcial, and J. McCloy, “Crystallization of iron-containing sodium aluminosilicate glasses in the $NaAlSiO_4$ -$NaFeSiO_4$ join,” *J. Geophys. Res. Solid Earth*, vol. 122, no. 4, pp. 2504–2524, Apr. 2017, doi: 10.1002/2016JB013661.

[2] A. Goel, J. S. McCloy, R. Pokorny, and A. A. Kruger, “Challenges with vitrification of Hanford High-Level Waste (HLW) to borosilicate glass – An overview,” *J. Non-Cryst. Solids X*, vol. 4, p. 100033, Dec. 2019, doi: 10.1016/j.nocx.2019.100033.

[3] J. Marcial, B. J. Riley, A. A. Kruger, C. E. Lonergan, and J. D. Vienna, “Hanford low-activity waste vitrification: A review,” *J. Hazard. Mater.*, vol. 461, p. 132437, Jan. 2024, doi: 10.1016/j.jhazmat.2023.132437.

[4] B. Cochain, D. R. Neuville, G. S. Henderson, C. A. McCammon, O. Pinet, and P. Richet, “Effects of the Iron Content and Redox State on the Structure of Sodium Borosilicate Glasses: A Raman, Mössbauer and Boron K-Edge XANES Spectroscopy Study,” *J. Am. Ceram. Soc.*, vol. 95, no. 3, pp. 962–971, Mar. 2012, doi: 10.1111/j.1551-2916.2011.05020.x.

[5] C. L. Pearce, K. M. Rosso, R. A. D. Pattrick, and A. R. Felmy, “Impact of iron redox chemistry on nuclear waste disposal,” in *Redox-reactive Minerals: Properties, Reactions and Applications in Clean Technologies*, 1st ed., I. A. M. Ahmed, Ed., Mineralogical Society of Great Britain & Ireland, 2007, pp. 229–272. doi: 10.1180/EMU-notes.17.7.

[6] K. A. Hudson-Edwards, *Redox-reactive Minerals: Properties, Reactions and Applications in Clean Technologies*, 1st ed. Mineralogical Society of Great Britain & Ireland, 2007. doi: 10.1180/EMU-notes.17.

[7] N. L. Bowen, J. Schairer, and H. W. V. Willems, “The ternary system; Na_2SiO_3 -Fe_2O_3 - SiO_2,” *American Journal of Science*, vol. 20, pp. 405–455, 1930.

[8] M. Ahmadzadeh, T. A. Olds, A. Scrimshire, P. A. Bingham, and J. S. McCloy, “Structure and properties of $Na_5FeSi_4O_{12}$ crystallized from $5Na_2O$–Fe_2O_3–$8SiO_2$ glass,” *Acta Crystallogr. Sect. C Struct. Chem.*, vol. 74, no. 12, pp. 1595–1602, Dec. 2018, doi: 10.1107/S2053229618014353.

[9] B. Maksimov, Y. A. Kharitonov, and N. Belov, "Crystal structure of the Na-Y metasilicate $Na_5YSi_4O_{12}$," *Sov. Physics—Doklady,* vol. 19, p. 763, 1974.
[10] A. Sivakumaran, A. J. Samson, and V. Thangadurai, “Progress in Sodium Silicates for All-Solid-State Sodium Batteries—a Review,” *Energy Technol.*, vol. 11, no. 4, p. 2201323, Apr. 2023, doi: 10.1002/ente.202201323.
[11] G. Sun *et al.*, “Electrochemically induced crystalline-to-amorphization transformation in sodium samarium silicate solid electrolyte for long-lasting sodium metal batteries,” *Nat. Commun.*, vol. 14, no. 1, p. 6501, Oct. 2023, doi: 10.1038/s41467-023-42308-0.
[12] A. Michalak, S. Behara, and A. R. M, “Reinvestigation of $Na_5GdSi_4O_{12}$: A Potentially Better Solid Electrolyte than Sodium β Alumina for Solid-State Sodium Batteries,” *ACS Appl. Mater. Interfaces*, vol. 16, no. 6, pp. 7112–7118, Feb. 2024, doi: 10.1021/acsami.3c16153.
[13] R. D. Shannon, B. E. Taylor, T. E. Gier, H. Y. Chen, and T. Berzins, “Ionic conductivity in sodium yttrium silicon oxide ($Na_5YSi_4O_{12}$)-type silicates,” *Inorg. Chem.*, vol. 17, pp. 958–964, 1978.
[14] R. D. Shannon, H.-Y. Chen, and T. Berzins, “Ionic Conductivity in $Na_5GdSi_4O_{12}$,” *Mat Res Bull*, vol. 12, pp. 969–973, 1977.
[15] D. Bailey and J. Schairer, “Crystallization of the rock-forming silicates in the system Na_2O-Fe_2O_3-Al_2O_3-SiO_2 at 1 atmosphere,” *1962-1963 Year Book - Carnegie Institution of Washington, vol. 62, Washington, D.C. : Carnegie Institution of Washington*, vol. 62, pp. 124–131, 1963.
[16] D. K. Bailey and J. F. Schairer, “The System Na_2O-Fe_2O_3-Al_2O_3-SiO_2 at 1 Atmosphere, and the Petrogenesis of Alkaline Rocks,” *J. Petrol.*, vol. 7, no. 1, pp. 114–170, Feb. 1966, doi: 10.1093/petrology/7.1.114.
[17] M. Ahmadzadeh *et al.*, “Structure of $NaFeSiO_4$, $NaFeSi_2O_6$, and $NaFeSi_3O_8$ glasses and glass-ceramics,” *Am. Mineral.*, vol. 105, no. 9, pp. 1375–1384, Sep. 2020, doi: 10.2138/am-2020-7285.
[18] J. S. McCloy, M. J. Schweiger, C. P. Rodriguez, and J. D. Vienna, “Nepheline Crystallization in Nuclear Waste Glasses: Progress Toward Acceptance of High-Alumina Formulations,” *Int. J. Appl. Glass Sci.*, vol. 2, no. 3, pp. 201–214, Sep. 2011, doi: 10.1111/j.2041-1294.2011.00055.x.
[19] P. Hrma, “Crystallization during processing of nuclear waste glass,” *J. Non-Cryst. Solids*, vol. 356, no. 52–54, pp. 3019–3025, Dec. 2010, doi: 10.1016/j.jnoncrysol.2010.03.039.
[20] F. Menges, *Spectragryph - optical spectroscopy software*. (2022).
[21] F. Baudelet *et al.*, “ODE: a new beam line for high-pressure XAS and XMCD studies at SOLEIL,” *High Press. Res.*, vol. 31, no. 1, pp. 136–139, Mar. 2011, doi: 10.1080/08957959.2010.532794.
[22] M. Newville, “Larch: An Analysis Package for XAFS and Related Spectroscopies,” *J. Phys. Conf. Ser.*, vol. 430, p. 012007, Apr. 2013, doi: 10.1088/1742-6596/430/1/012007.
[23] M. Wilke, F. Farges, P.-E. Petit, G. E. Brown, and F. Martin, “Oxidation state and coordination of Fe in minerals: An Fe *K*-XANES spectroscopic study,” *Am. Mineral.*, vol. 86, no. 5–6, pp. 714–730, May 2001, doi: 10.2138/am-2001-5-612.
[24] M. Wilke, G. M. Partzsch, R. Bernhardt, and D. Lattard, “Determination of the iron oxidation state in basaltic glasses using XANES at the K-edge,” *Chem. Geol.*, vol. 213, no. 1–3, pp. 71–87, Dec. 2004, doi: 10.1016/j.chemgeo.2004.08.034.
[25] B. H. Toby and R. B. Von Dreele, “*GSAS-II* : the genesis of a modern open-source all purpose crystallography software package,” *J. Appl. Crystallogr.*, vol. 46, no. 2, pp. 544–549, Apr. 2013, doi: 10.1107/S0021889813003531.

[26] J. J. Donovan, *Probe for EPMA v. 10.4.5, User's Guide and Reference, Xtreme Edition*. 2014.
[27] R. Pokorný *et al.*, "Transient melt formation and its effect on conversion phenomena during nuclear waste vitrification – HT-ESEM analysis," *J. Am. Ceram. Soc.*, vol. 107, no. 3, pp. 1691–1705, Mar. 2024, doi: 10.1111/jace.19361.
[28] D. Kelly, "Analysis of geological materials by low dilution fusion at the Peter Hooper Geoanalytical Lab (Washington State University)," Dec. 2018, Accessed: Jul. 23, 2024. [Online]. Available: https://hdl.handle.net/2376/101916.
[29] Z. Jia, C. Liu, C. Niu, K. Li, and K. Xu, "Volatilization of sodium and boron from nuclear waste glass and associated effects on glass structure and thermal stability," *J. Nucl. Mater.*, vol. 587, p. 154712, Dec. 2023, doi: 10.1016/j.jnucmat.2023.154712.
[30] J. S. McCloy, N. Smith-Gray, J. M. Bussey, N. Stone-Weiss, and R. E. Youngman, "Fluorine in Complex Alumino-Boro-Silicate Glasses: Insight into Chemical Environment and Structure," *Inorg. Chem.*, vol. 63, no. 10, pp. 4669–4680, Mar. 2024, doi: 10.1021/acs.inorgchem.3c04281.
[31] M. Edén, "Update on ^{27}Al NMR studies of aluminosilicate glasses," in *Annual Reports on NMR Spectroscopy*, vol. 101, Elsevier, 2020, pp. 285–410. doi: 10.1016/bs.arnmr.2020.07.002.
[32] B. Hehlen, E. Courtens, A. Yamanaka, and K. Inoue, "Nature of the Boson peak of silica glasses from hyper-Raman scattering," *J. Non-Cryst. Solids*, vol. 307–310, pp. 87–91, Sep. 2002, doi: 10.1016/S0022-3093(02)01444-8.
[33] D. A. McKeown, F. L. Galeener, and G. E. Brown, "Raman studies of Al coordination in silica-rich sodium aluminosilicate glasses and some related minerals," *J. Non-Cryst. Solids*, vol. 68, no. 2–3, pp. 361–378, Nov. 1984, doi: 10.1016/0022-3093(84)90017-6.
[34] A.-M. Welsch, J. L. Knipping, and H. Behrens, "Fe-oxidation state in alkali-trisilicate glasses - A Raman spectroscopic study," *J. Non-Cryst. Solids*, vol. 471, pp. 28–38, Sep. 2017, doi: 10.1016/j.jnoncrysol.2017.04.033.
[35] K. Baert *et al.*, "Using Raman spectroscopy as a tool for the detection of iron in glass," *J. Raman Spectrosc.*, vol. 42, no. 9, pp. 1789–1795, Sep. 2011, doi: 10.1002/jrs.2935.
[36] M. I. Tuheen, M. C. Wilkins, J. McCloy, and J. Du, "The structures of iron silicate glasses with varying iron redox ratios from molecular dynamics simulations and EXAFS analysis," *J. Non-Cryst. Solids*, vol. 624, p. 122713, Jan. 2024, doi: 10.1016/j.jnoncrysol.2023.122713.
[37] R. O. Sack, I. S. E. Carmichael, M. Rivers, and M. S. Ghiorso, "Ferric-ferrous equilibria in natural silicate liquids at 1 bar," *Contrib. Mineral. Petrol.*, vol. 75, no. 4, pp. 369–376, Feb. 1981, doi: 10.1007/BF00374720.
[38] H. Li, P. Hrma, J. D. Vienna, M. Qian, Y. Su, and D. E. Smith, "Effects of Al_2O_3, B_2O_3, Na_2O, and SiO_2 on nepheline formation in borosilicate glasses: chemical and physical correlations," *J. Non-Cryst. Solids*, vol. 331, no. 1–3, pp. 202–216, Dec. 2003, doi: 10.1016/j.jnoncrysol.2003.08.082.
[39] R. J. Kirkpatrick, "Crystal Growth from melt: a review," *American Mineralogist*, vol. 60, pp. 798–814, 1975.
[40] N. Pathak, S. K. Gupta, K. Sanyal, M. Kumar, R. M. Kadam, and V. Natarajan, "Photoluminescence and EPR studies on Fe^{3+} doped $ZnAl_2O_4$: an evidence for local site swapping of Fe^{3+} and formation of inverse and normal phase," *Dalton Trans.*, vol. 43, no. 24, p. 9313, 2014, doi: 10.1039/c4dt00741g.